Proceedings Paper:
Delis, I, Dmochowski, JP, Sajda, P et al. (2018) Correlations of Neural Activity with Behavioral Kinematics during Active Tactile Decision Making. In: Proceedings of the 10th Hellenic Conference on Artificial Intelligence. SETN 2018: 10th Hellenic Conference on Artificial Intelligence, 09-12 Jul 2018, Patras, Greece. ACM. Article no: 25. ISBN: 978-1-4503-6433-1.

https://doi.org/10.1145/3200947.3201027

Correlations of Neural Activity with Behavioral Kinematics during Active Tactile Decision Making

Full Paper

Ioannis Delis
Department of Biomedical Sciences
University of Leeds
Leeds, LS2 9JT, UK
i.delis@leeds.co.uk

Jacek P Dmochowski
Department of Biomedical Engineering
City College of New York
New York, NY 10031, USA
jdmochowski@ccny.cuny.edu

Paul Sajda
Department of Biomedical Engineering
Columbia University
New York, NY 10027, USA
psajda@columbia.edu

Qi Wang
Department of Biomedical Engineering
Columbia University
New York, NY 10027, USA
psajda@columbia.edu

ABSTRACT

Most real-world decisions rely on active sensing, a dynamic process for directing our sensors (e.g. eyes or fingers) across a stimulus in order to reduce uncertainty and maximize information gain. Though ecologically pervasive, relatively limited work has focused on identifying neural correlates of the active sensing process. In tactile perception, we often make decisions about an object or surface by actively exploring its shape and texture. Here we investigate the neural mechanisms of active tactile sensing by simultaneously measuring electroencephalography (EEG) and finger kinematics while subjects interrogated a haptic surface to make perceptual judgements. We hypothesized that one's sensorimotor behavior provides a view into the cognitive processes leading to decision formation, and the neural correlates of these processes would be detectable by relating kinematics to neural activity. Using an adaptation of canonical correlation analysis (CCA), we regressed the EEG onto kinematics and found three distinct, task-related EEG components that localized to right-lateralized occipital cortex (LOC), middle frontal gyrus (MFG), and supplementary motor area (SMA), respectively. To probe the functional role of these components, we fit their single-trial activity to behavior using a hierarchical drift diffusion model (HDDM), revealing that the LOC modulated the encoding of the tactile stimulus whereas the MFG predicted the rate of information integration towards a choice. This study provides direct evidence that, how we explore the stimulus yields insight into how our brain is forming a decision and uncovers the neural correlates of distinct sensory encoding and evidence accumulation processes during active tactile sensing.

KEYWORDS

Active tactile sensing, perceptual decision making, EEG, pantograph, canonical correlation analysis, hierarchical drift diffusion model

1 INTRODUCTION

Perceptual decisions rely on the integration of sensory evidence from the environment [1]. The quality of sensory evidence depends highly on our actions, as our movements affect how we sample, process and integrate information from the external world [2-4]. Hence, to optimize the speed and accuracy of our perceptual decisions we need to direct our actions so as to efficiently gather sensory information, a process called active sensing [5]. Importantly, the processing of sensory information acquired actively and its translation into perceptual choices requires the interaction of multiple neural processes (and consequently multiple brain areas) over time [6-8]. However, despite recent interest in active sensing and decision-making, its neural underpinnings remain elusive.

Here we address this gap using a response-time active tactile decision-making task in which we simultaneously measured the electroencephalogram (EEG), sensorimotor behavior (movement

SETN '18, July 9–15, 2018, Rio Patras, Greece

ACM ISBN 978-1-4503-6433-1/18/07..$15.00
https://doi.org/10.1145/3200947.3201006

kinematics) and task performance (accuracy and response time - RT) of subjects, the goal being to uncover the neural and sensorimotor mechanisms underlying active perceptual decisions (see Figure 1 for a schematic illustration of the computational methodology we employed here).

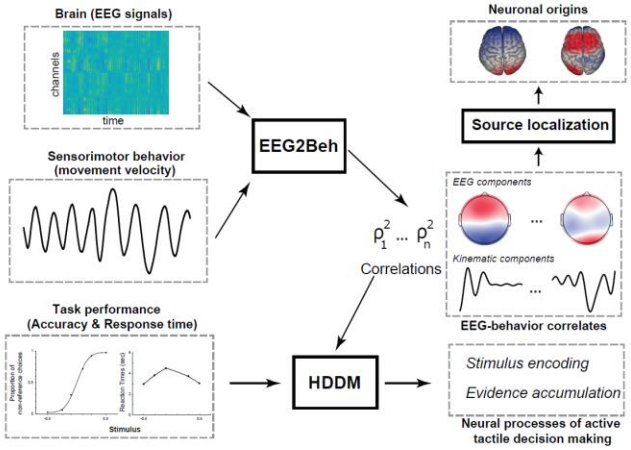

Figure 1. Illustration of the analysis framework implemented in this study. To characterize active tactile decision-making, three types of measurements are simultaneously made: a) EEG recordings, b) sensorimotor signals (movement kinematics), and c) task performance measures (accuracy and response time - RT). EEG and kinematic signals are input to the EEG2Beh algorithm that outputs pairs of brain – behavior coupling components (scalp maps and temporal kinematic filters) and their correlation measures ρ^2. The brain (EEG) components are input to a source localization algorithm to identify their neuronal origins. The EEG2Beh coupling strengths ρ^2 inform the hierarchical drift diffusion modelling (HDDM) of the task performance data. HDDM uses the ρ^2 to translate accuracy and RT into the components of decision-making processing (such as evidence accumulation or stimulus encoding) thereby characterizing the functional role of each EEG2Beh component.

In addition to this, complex periodic arrays of dipolarly coupled magnetic dots are of special interest because they can support the propagation of non-reciprocal spin waves, i.e. (□(*k*) ≠ □ (−*k*)), where □ is the angular frequency and *k* is a wave vector, which could find application in the signal transmission and information processing as well as in the design of microwave isolators and circulators.

2 EXPERIMENTAL PROCEDURES

2.1 Tactile Texture Discrimination Task

Fifteen healthy right-handed subjects (6 female, aged 26±2 years) performed a two-alternative forced choice (2AFC) texture discrimination task during which they compare the amplitudes of two sinusoidal textures of the same frequency. experimental procedures have been approved by the Institutional Review Board (IRB) at Columbia University.

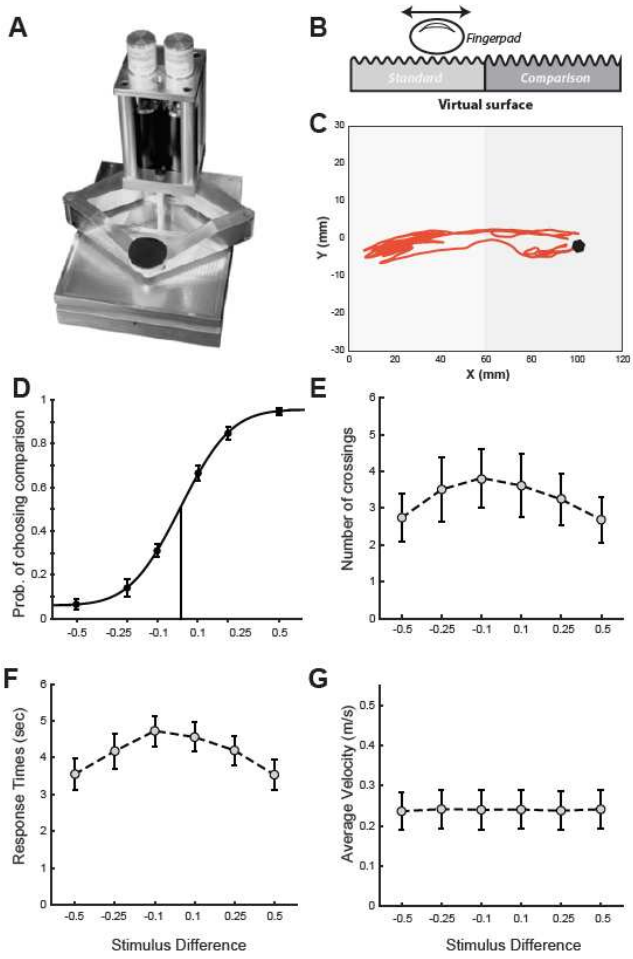

Figure 2. Experimental design and behavioral results. A. The Pantograph is a haptic device used to render virtual surfaces that can be actively sensed. B. The stimulus. We programmed the Pantograph to generate a virtual grating texture. The workspace was split into two subspaces (left - L and right - R) that differed in the amplitude of the virtual surface that the subjects actively sensed. One of the two sides (randomly assigned) had the reference amplitude (equal to 1) and the other had the comparison amplitude that varied on each trial taking one of the values: 0.5, 0.75, 0.9, 1.1, 1.25, and 1.5. C. Index finger trajectory indicating the scanning pattern of the virtual texture in one trial. The two red dots indicate the starting point and endpoint. On this trial, the subject actively sensed the left subspace first, then moved to the right subspace and explored it before coming back to the left subspace again and reporting their choice. D. Psychometric curve indicating the percentage of non-reference choices for all stimulus differences. Dots indicate average proportion of choices across subjects and errorbars are standard error of the means (sem) across subjects. Data are fit using a cumulative Gaussian function. E. Number of crossings (i.e. switchings between the two stimuli) shown as averages (± sem) across subjects. F. Response times for all stimulus differences shown as averages (± sem) across subjects. G. Average finger velocities for all stimulus differences (mean ± sem across subjects).

Subjects performed the task using a haptic device, called a Pantograph [9], which can be judiciously programmed to generate tactile sensations that resemble exploring real surfaces. For this binary discrimination task, the workspace of the Pantograph (of dimensions 110mm x 60mm) was split into two subspaces (left - L and right - R, 55mm x 60 mm each) and subjects were asked to report as quickly and as accurately as possible which of the two subspaces had the higher texture amplitude. Subjects placed their index finger on the plate of the Pantograph and were allowed to move it freely in the Pantograph workspace to explore the textures of both subspaces before reporting their choice by pressing one of two buttons on a keyboard (left arrow for L, right arrow for R). Subjects experienced continuous sinusoidal forces of different amplitudes (but same frequency) in the two subspaces.

On each trial, subjects compared between the reference amplitude 1 (presented either on the left or right subspace) and one of six other amplitude levels (0.5, 0.75, 0.9, 1.1, 1.25, 1.5). Each subject performed 20 trials for each amplitude level, resulting in 20 trials x 6 amplitudes = 120 trials in total. The full experiment was split into 3 blocks of 40 trials. Subjects were not able to see their moving right hand (and index finger) while performing the task. One subject showed poor behavioral performance (accuracy was not significantly different from chance level) and another subject's EEG recordings were significantly contaminated with eye movement artifacts, thus data from these two subjects were removed from any subsequent analyses. We report results from the remaining 13 subjects.

2.2 Data Recording and Pre-processing

Movement kinematics (x, y coordinates of finger position) and applied forces were measured at a sampling frequency of 1000Hz. Single-trial movement velocity waveforms were computed using the derivatives of the recorded position. During performance of the task, we also recorded EEG signals at 2048 sampling frequency using a Biosemi EEG system (ActiveTwo AD-box, 64 Ag-AgCl active electrodes, 10-10 montage). EEG recordings were preprocessed using EEGLab [10] as follows. EEG signals were first down-sampled to 1000Hz to match movement kinematics and dynamics. Then, they were bandpass filtered to 1-50Hz using a Hamming windowed FIR filter. To isolate the purely neural component of the EEG data, we used the following procedure: we first reduced the dimensionality of the EEG data by reconstituting the data using only the top 32 principal components derived from Principal Component Analysis (PCA). Thereafter, an Independent Component Analysis (ICA) decomposition of the data was performed using the Infomax algorithm [11]. We then used an ICA-based artifact removal algorithm called MARA [12] to remove ICs attributed to blinks, horizontal eye movements (HEOG), muscular activity (EMG), and any highly noisy electrodes. We removed components with probabilities of being artifacts above 0.5.

3 DATA ANALYSIS & MODELING

3.1 EEG2Behavior Analysis

Eavesdropping. To identify correlations between the EEG recordings and the subjects' active sensory experience, we used a novel methodology, termed EEG2Beh(aviour). EEG2Beh extends the previously developed Stim2EEG [13] to make it applicable to simultaneously recorded neural activity and sensorimotor behavioral signals. The method is based on the temporal filtering of the velocity signals *s(t)* and the spatial integration of *i* EEG signals $m_i(t)$ (Fig. 3):

$$u(t) = h(t) * s(t)\,,$$
$$v(t) = \sum_i g_i m_i(t) \qquad (1)$$

The temporal filter *h(t)* and spatial filter g_i are found by maximizing the correlation $\rho(u, v)$ between the filtered movement velocity *u(t)* and the filtered EEG activity *v(t)*:

$$\rho(u, v) = \frac{\sum_t u(t)v(t)}{\sqrt{\sum_t u^2(t)v^2(t)}} \qquad (2)$$

To learn the filters that yield maximally correlated EEG and kinematic components, we performed Canonical Correlation Analysis [14] (CCA), which provides multiple pairs of covariates. Each pair *c* captures in g_{ci} a spatial filter of EEG activity and in $h_c(t)$ a temporal filter of the movement velocity. Here we chose the temporal aperture of the temporal filters to be [-1s,1s] (varying the filter aperture did not change qualitatively the results). To visualize the spatial distribution of neural activity associated with each filter, we computed the EEG components w using the "forward model" formalism as follows [15-17]:

$$W = R_{mm}G(G^T R_{mm}G)^{-1} \qquad (3)$$

where R_{mm} is the autocovariance matrix of the EEG data matrix $M = [m_1, m_2, \cdots, m_I]$ and $G = [g_1, g_2, \cdots, g_C]$ is a matrix of the *C* CCA-derived spatial filters. The corresponding forward models are the columns of matrix $W = [w_1, w_2, \cdots, w_C]$. Hence this approach extracts *C* pairs of temporal kinematic components and spatial EEG components $(h_t, w_s)_i$ that correlate with strength ρ_i in decreasing order $\rho_1 > \rho_2 > \cdots > \rho_C$.

To determine statistical significance of the correlations at each learned component pair ($\rho_k > 0$), we randomized the phase spectrum of the EEG signals, which disrupted the temporal relationship between the EEG activity and the kinematics while preserving the autocorrelation structure of the signals [18]. We generated 1000 phase-randomized surrogates of the EEG data and computed EEG2Beh correlations with kinematics to define the null distribution from which we estimated p-values. In contrast to a standard shuffling procedure that disrupts any coordination across EEG sensors, this phase-randomization procedure maintains the magnitude spectrum of the EEG signals, thus conserving their autocorrelation structure, which is a fundamental feature of the original signals when the significance of cross-correlation is assessed. Hence, using this procedure, the obtained surrogates that define the null distribution are a more plausible comparison (resulting in a stricter statistical test) than randomly shuffled surrogates. This procedure gave *c=3* significant components.

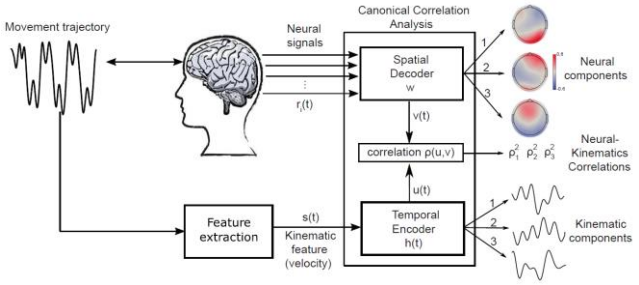

Figure 3. Schematic view of EEG2Beh(avior). Subjects move their fingers to actively sense a surface while their brain activity (e.g. EEG signals) $r_i(t)$ is recorded. The relevant kinematic features of the sensorimotor behavior (for example, the movement velocity) are extracted, resulting in a time series s(t). An optimization procedure, implemented via canonical correlation analysis, then computes spatial filters w to apply to the neural signals and temporal filters h(t) to apply to the kinematic features such that the resulting filter outputs are maximally correlated in time. The algorithm output is a set of kinematic and EEG components and their coupling strengths ρ^2.

3.2 Source Localization

To identify the brain regions that generated the EEG component activations we performed a source reconstruction analysis. We used Brainstorm [19], an open-source Matlab package for M/EEG signal processing, to translate the obtained forward models into distributions of underlying cortical activity. A standardized head model based on the average template brain of the Montreal Neurological Institute was used as single subject MRI data were not available. To estimate the sources, we used the whitened and depth-weighted linear L2-minimum norm estimates algorithm with no noise modelling (noise covariance equal to the identity matrix) and estimated amplitude SNR of the recordings equal to 3 (default - used to compute the regularization parameter). We constrained the orientation of the source model by modelling at each grid point only one dipole that is oriented normally to the cortical surface.

3.3 Hierarchical Drift Diffusion Modelling of Performance Data with EEG2Beh Regressors.

We fit the subjects' performance, i.e. accuracy and response time (RT), with a hierarchical drift diffusion model (HDDM) [20] which assumes a stochastic accumulation of sensory evidence over time, toward one of two decision boundaries corresponding to correct and incorrect choices [21, 22]. The model returns estimates of internal components of processing such as the rate of evidence accumulation (drift rate), the distance between decision boundaries controlling the amount of evidence required for a decision (decision boundary), a possible bias towards one of the two choices (starting point) and the duration of non-decision processes (non-decision time), which include stimulus encoding and response production. As per common practice, we assumed that stimulus differences affected the drift rate [23].

In short, the model iteratively adjusts the above parameters to maximize the summed log likelihood of the predicted mean response time (RT) and accuracy. The DDM parameters were estimated in a hierarchical Bayesian framework, in which prior distributions of the model parameters were updated on the basis of the likelihood of the data given the model, to yield posterior distributions [20, 24, 25]. The use of Bayesian analysis, and specifically hierarchical Bayesian analysis has several benefits relative to traditional DDM analysis. First, posterior distributions directly convey the uncertainty associated with parameter estimates [26, 27]. Second, the Bayesian hierarchical framework has been shown to be especially effective when the number of observations is low [28]. Third and more importantly, this framework supports the use of other variables as regressors of the model parameters to assess relations of the model parameters with other physiological or behavioral data [29-32]. This property of the HDDM allowed us to establish the link between the results of the brain-behavior coupling analysis and the model parameters.

To implement the hierarchical DDM, we used the JAGS Wiener module [20] in JAGS [33], via the Matjags interface in Matlab to estimate posterior distributions. For each trial, the likelihood of accuracy and RT was assessed by providing the Wiener first-passage time (WFPT) distribution with the four model parameters (boundary separation, starting point, non-decision time, and drift rate). Parameters were drawn from uniformly distributed priors and were estimated with non-informative mean and standard deviation group priors. The starting point was set as the midpoint between the two decision boundaries as the experimental design induced no bias towards one of the two choices [34]. There were 5,500 samples drawn from the posterior; the first 500 were discarded (as "burn-in") and the rest were subsampled ("thinned") by a factor of 50 following the conventional approach to MCMC sampling whereby initial samples are likely to be unreliable due to the selection of a random starting point and neighboring samples are likely to be highly correlated [20, 24].

We used the single-trial EEG2Beh correlations of the identified components as regressors of the decision parameters (non-decision time, τ and drift rate, δ) as follows:

$$\tau = \beta_0 + \beta_1 * \rho_1^2 + \beta_2 * \rho_2^2 + \beta_3 * \rho_3^2 \quad (4)$$

$$\delta = \gamma_0 + \gamma_1 * \rho_1^2 + \gamma_2 * \rho_2^2 + \gamma_3 * \rho_3^2 \quad (5)$$

In these regressions, ρ_i^2 are the squared single-trial EEG2Beh correlations of the three components respectively. The coefficients β_i (γ_i) weight the slope of the non-decision time (drift rate) by the values of ρ_i^2 on that specific trial, with an intercept β_0 (γ_0). By using these eight regression coefficients we were able to test the influences of each of the three identified components on either of the model parameters [29].

For comparison with alternate models, we used the Deviance Information Criterion (DIC), a measure widely used for fit assessment and comparison of hierarchical models [35]. DIC selects the model that achieves the best trade-off between goodness-of-fit and model complexity. Lower DIC values favour models with the highest likelihood and least degrees of freedom.

4 RESULTS

To generate tactile stimulation that can be actively sensed, we employed a haptic device, called the Pantograph [9](Figure 2A) and programmed it to render a virtual grating texture with different amplitudes (Figure 2B-C). On each trial, subjects compared a reference texture amplitude (which was randomly presented in one of the two regions) and a comparison texture with higher or lower amplitude (six amplitude differences: -0.5, -0.25, -0.1, 0.1, 0.25. 0.5). Task performance improved significantly with increasing stimulus difference, as reflected by a larger fraction of correct choices ($p<10^{-7}$, F(2, 36)=27.03) and faster RTs ($p<0.05$, F(2, 36)=4.04) (Figure 2D-F).

During this active tactile decision-making task, we also recorded a) the subjects' finger position, offering a detailed account of their active sensing strategy and b) their EEG activity reflecting the neural dynamics that underlie performance of this task. First, we examined what aspects of the active sensing strategy used by the subjects were affected by task difficulty. We found that smaller stimulus differences resulted in more crossings, i.e. the harder the task, the more times the subjects switched between the two textures in order to compare their amplitudes (although this difference was not significant, $p=0.17$, F(2,36)=1.87, Figure 2E). Interestingly, the average speed with which the subjects scanned the textures was independent of the stimulus difference (Figure 2G).

After characterizing the subjects' behavioral performance, we then probed the relationship between the subjects' active sensory experience and their brain activity. To this end, we implemented a novel analytical method termed "EEG2Beh(avior)". EEG2Beh aims to identify maximally correlated components of brain – sensorimotor behavior coupling using an optimization procedure based on Canonical Correlation Analysis (CCA) [14].

To identify EEG2Beh components that describe performance of this task consistently across subjects, we pooled the pre-processed EEG and velocity data across all subjects and applied them to the EEG2Beh algorithm. The algorithm extracted three pairs of prominent EEG (spatial) and kinematic (temporal) components (Figure 3) showing significant EEG2Beh coupling (rho=0. $p<0.05$, corrected for multiple comparisons using Bonferroni correction). The first EEG component was distributed over multiple right-lateralized occipito-parietal electrode locations (high positive activations). Source localization of the EEG component revealed a neuronal origin in the right lateral occipital complex (LOC) (Figure 4). The second EEG component was focused over right prefrontal electrodes and its brain source was localized to the right middle frontal gyrus (MFG). The topography of the third EEG component showed high positive activations over frontal and central electrodes and negative activations over occipital electrode locations. Source reconstruction placed the origin of this component in the premotor cortex and supplementary motor area (SMA).

Having specified the main components of brain activity and active sensing behavior that describe this task, we then aimed to establish the missing link between this brain-behavior coupling and decision-making performance. We asked whether trial-to-trial fluctuations in the brain-behavior coupling have a direct influence on behaviour and, in particular, which decision-making processes they may be implicated in. To address this question, we first quantified the brain-behavior coupling in single trials, i.e. computed single-trial ρ^2 values by filtering the single-trial EEG and kinematic data with the identified spatial and temporal filters respectively. Then, we integrated the single-trial ρ^2 values into a hierarchical drift diffusion model (HDDM) [22, 24], a cognitive model of decision-making behavior that decomposes task performance, i.e. accuracy and RT, into the internal components of processing.

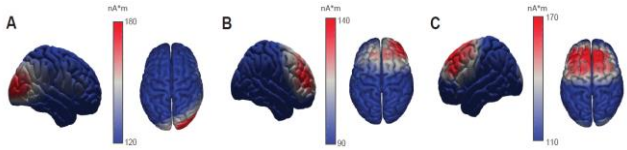

Figure 4. Brain sources of the three EEG components.

Within the HDDM framework, we estimated regression coefficients (β, γ) to determine the relationship between trial-to-trial variations in ρ^2 and the main decision parameters (see Figure 5A for a graphical illustration of the model). We found that the brain-behavior correlations of the first (occipital) component were significantly negatively correlated to the non-decision times ($p<0.01$, the stronger the coupling the shorter the non-decision times, Figure 5B) and the correlations of the second (prefrontal) component were predictive of the drift rate ($p<0.01$, higher drift rates for stronger couplings, Figure 5C), whereas the third component did not show any significant relation to the HDDM parameters.

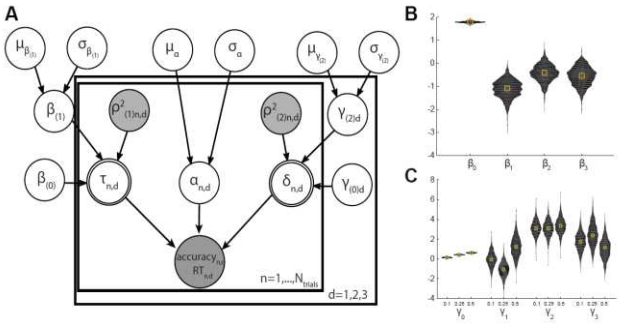

Figure 5. HDDM formulation and regression results. A. Graphical model showing hierarchical estimation of Drift Diffusion Model parameters with EEG2Beh regressors. Round nodes represent continuous random variables and double-bordered nodes represent deterministic variables, defined in terms of other variables. Shaded nodes represent recorded or computed signals, including single-trial behavioral data (accuracy, RT) and EEG2Beh coupling measures (ρ^2). Open nodes represent unobserved latent parameters. Parameters are modelled as random variables with inferred means μ and variances σ^2. Plates denote that multiple random variables share the same parents and children. The outer plate is over difficulty levels d while the inner plate is over trials n. For

example, each single-trial boundary separation $a_{n,d}$ shares the same parents μ_α and σ_α^2 that define the distribution across trials and difficulty levels. Single-trial variations of non-decision time τ and drift rate δ are determined by EEG2Beh couplings with regression coefficients β and γ. B. Violin plots showing the distribution of the regression coefficients β_i for the prediction of single-trial non-decision times τ. C. Violin plots showing the distribution of the regression coefficients γ for the prediction of single-trial drift rates δ.

5 DISCUSSION

In this study, we probed the mechanisms underlying active perceptual decisions and showed that the sensorimotor strategy employed for active sensing determines the reliability of the decision formation processes. In particular, the quality of tactile stimulus encoding and evidence accumulation pertain to the coupling between the kinematic patterns of the subject's motion and the neural activity that drives (and is driven by) this motion. The significance of our approach and the implications of the findings is discussed in the following.

5.1 Active Sensing as a Window into the Neural Processes of decision-making.

There has been significant progress in the study of the neural processes of perceptual decision-making [8, 36]. However, in most decision-making research, sensory information sampling, processing, and integrating takes place passively, whereas in real-world settings most perceptual decisions are made during active behaviors (e.g eye movements to gather information about a visual stimulus [37] or hand/finger movements to explore a tactile surface [38]). This process entails the integration of information from multiple locations in order to both select the next movement and solve the task [4]. Hence, a closed-loop sensorimotor strategy is implemented in order to acquire the necessary evidence [2, 3, 5]. Here we investigated this sensorimotor loop using a novel approach which decodes a pattern of neural activity that encodes a pattern of the movement kinematics.

5.2 A Distributed Neural Network For Active Perceptual Decision-Making.

We found that three kinematic patterns are encoded in different brain regions and the respective brain-behavior coupling was predictive of dissociable decision-making processes. First, right occipital cortical activity was shown to modulate the non-decision time duration of the decision formation procedure. This parameter includes the durations of a) the stimulus encoding and b) the motor response to indicate the choice made. From these two processes, the latter is not expected to vary significantly from trial to trial in this experimental paradigm and furthermore, motor actions are not localized in occipital areas. Hence, we deduce that the occipital component likely represents the fidelity of tactile sensory encoding. Second, we found that the component localizing to prefrontal cortex was predictive of the rate of evidence accumulation towards a tactile decision, which is also compatible with previous work [39]. We also identified a third component localizing to the supplementary motor area that showed significant EEG-kinematics coupling but did not correlate with any DDM model parameter. SMA is known to participate in producing motor behavior and has been previously demonstrated to be involved in tactile decision-making. Taken together, our results suggest that active perceptual decisions are based on the interaction of different neural networks with complementary roles [8].

5.3 Informed Cognitive Modeling to Uncover Latent Neural Processes.

An important contribution of our study is the dissociation of the roles of the identified neural/kinematic patterns. This was only made possible by the joint cognitive modeling of behavioral and neural/kinematic data that linked the neural correlates of sensori-motor behavior with the higher cognitive processes involved in decision-making. Similar model-based cognitive neuroscience approaches have been proposed recently and have been shown to be effective in characterizing the neural underpinnings of behavioral components [32]. Here we found that the subjects' cognitive state on each trial - as reflected by trial-to-trial variability of the brain-behavior coupling in a) occipital and b) prefrontal cortices – indexes the reliability of a) sensory encoding and b) integration of perceptual information.

ACKNOWLEDGMENTS

This work was supported by the National Institutes of Health under Grant R01-MH085092, the U.S. Army Research Laboratory under Cooperative Agreement W911NF-10-2-0022 and the UK Economic and Social Research Council under grant number ES/ L012995/1 to P.S., and a NARSAD Young Investigator award to Q.W..

REFERENCES

[1] Heekeren, H. R., Marrett, S., Bandettini, P. A. and Ungerleider, L. G. A general mechanism for perceptual decision-making in the human brain. Nature, 431, 7010 (Oct 14 2004), 859-862.

[2] Schroeder, C. E., Wilson, D. A., Radman, T., Scharfman, H. and Lakatos, P. Dynamics of Active Sensing and perceptual selection. Curr Opin Neurobiol, 20, 2 (Apr 2010), 172-176.

[3] Yang, S. C., Lengyel, M. and Wolpert, D. M. Active sensing in the categorization of visual patterns. eLife, 5(Feb 10 2016).

[4] Chukoskie, L., Snider, J., Mozer, M. C., Krauzlis, R. J. and Sejnowski, T. J. Learning where to look for a hidden target. Proc Natl Acad Sci U S A, 110 (Jun 18 2013), 10438-10445.

[5] Yang, S. C. H., Wolpert, D. M. and Lengyel, M. Theoretical perspectives on active sensing. Curr Opin Behav Sci, 11(Oct 2016), 100-108.

[6] Summerfield, C. and de Lange, F. P. Expectation in perceptual decision making: neural and computational mechanisms. Nat Rev Neurosci, 15, 11 (Nov 2014), 745-756.

[7] Philiastides, M. G. and Sajda, P. EEG-informed fMRI reveals spatiotemporal characteristics of perceptual decision making. J Neurosci, 27, 48 (Nov 28 2007), 13082-13091.

[8] Heekeren, H. R., Marrett, S. and Ungerleider, L. G. The neural systems that mediate human perceptual decision making. Nat Rev Neurosci, 9, 6 (Jun 2008), 467-479.

[9] Campion, G., Wang, Q. and Hayward, V. The Pantograph Mk-II: A haptic instrument. 2005 Ieee/Rsj International Conference on Intelligent Robots and Systems, Vols 1-4 2005, 723-728.

[10] Delorme, A. and Makeig, S. EEGLAB: an open source toolbox for analysis of single-trial EEG dynamics including independent component analysis. J Neurosci Meth, 134, 1 (Mar 15 2004), 9-21.
[11] Bell, A. J. and Sejnowski, T. J. An information-maximization approach to blind separation and blind deconvolution. Neural Comput, 7, 6 (Nov 1995), 1129-1159.
[12] Winkler, I., Haufe, S. and Tangermann, M. Automatic classification of artifactual ICA-components for artifact removal in EEG signals. Behavioral and brain functions, 7(Aug 02 2011), 30.
[13] Dmochowski, J. P., Ki, J. J., DeGuzman, P., Sajda, P. and Parra, L. C. Extracting multidimensional stimulus-response correlations using hybrid encoding-decoding of neural activity. NeuroImage(May 22 2017).
[14] Hotelling, H. Relations between two sets of variates. Biometrika, 28(Dec 1936), 321-377.
[15] Parra, L., Alvino, C., Tang, A., Pearlmutter, B., Yeung, N., Osman, A. and Sajda, P. Linear spatial integration for single-trial detection in encephalography. NeuroImage, 17, 1 (Sep 2002), 223-230.
[16] Parra, L. C., Spence, C. D., Gerson, A. D. and Sajda, P. Recipes for the linear analysis of EEG. NeuroImage, 28, 2 (Nov 01 2005), 326-341.
[17] Haufe, S., Meinecke, F., Gorgen, K., Dahne, S., Haynes, J. D., Blankertz, B. and Biessmann, F. On the interpretation of weight vectors of linear models in multivariate neuroimaging. NeuroImage, 87(Feb 15 2014), 96-110.
[18] Theiler, J., Eubank, S., Longtin, A., Galdrikian, B. and Farmer, J. D. Testing for Nonlinearity in Time-Series - the Method of Surrogate Data. Physica D, 58, 1-4 (Sep 15 1992), 77-94.
[19] Tadel, F., Baillet, S., Mosher, J. C., Pantazis, D. and Leahy, R. M. Brainstorm: a user-friendly application for MEG/EEG analysis. Computational intelligence and neuroscience, 2011), 879716.
[20] Wabersich, D. and Vandekerckhove, J. Extending JAGS: A tutorial on adding custom distributions to JAGS (with a diffusion model example). Behav Res Methods, 46, 1 (Mar 2014), 15-28.
[21] Ratcliff, R. A diffusion model account of response time and accuracy in a brightness discrimination task: Fitting real data and failing to fit fake but plausible data. Psychonomic bulletin & review, 9, 2 (Jun 2002), 278-291.
[22] Ratcliff, R. and McKoon, G. The diffusion decision model: Theory and data for two-choice decision tasks. Neural Computation, 20, 4 (Apr 2008), 873-922.
[23] Ratcliff, R. and Frank, M. J. Reinforcement-based decision making in corticostriatal circuits: mutual constraints by neurocomputational and diffusion models. Neural Comput, 24, 5 (May 2012), 1186-1229.
[24] Wiecki, T. V., Sofer, I. and Frank, M. J. HDDM: Hierarchical Bayesian estimation of the Drift-Diffusion Model in Python. Frontiers in neuroinformatics, (72013), 14.
[25] Kruschke, J. K. Bayesian data analysis. Wires Cogn Sci, 1, 5 (Sep-Oct 2010), 658-676.
[26] Kruschke, J. K. What to believe: Bayesian methods for data analysis. Trends in Cognitive Sciences, 14, 7 (Jul 2010), 293-300.
[27] Gelman, A. A Bayesian formulation of exploratory data analysis and goodness-of-fit testing. Int Stat Rev, 71, 2 (Aug 2003), 369-382.
[28] Ratcliff, R. and Childers, R. Individual Differences and Fitting Methods for the Two-Choice Diffusion Model of Decision Making. Decision, 2015.
[29] Cavanagh, J. F., Wiecki, T. V., Kochar, A. and Frank, M. J. Eye tracking and pupillometry are indicators of dissociable latent decision processes. Journal of experimental psychology. General, 143, 4 (Aug 2014), 1476-1488.
[30] Frank, M. J., Gagne, C., Nyhus, E., Masters, S., Wiecki, T. V., Cavanagh, J. F. and Badre, D. fMRI and EEG predictors of dynamic decision parameters during human reinforcement learning. J Neurosci, 35, 2 (Jan 14 2015), 485-494.
[31] Nunez, M. D., Vandekerckhove, J. and Srinivasan, R. How attention influences perceptual decision making: Single-trial EEG correlates of drift-diffusion model parameters. Journal of Mathematical Psychology, 76(Feb 2017), 117-130.
[32] Turner, B. M., van Maanen, L. and Forstmann, B. U. Informing Cognitive Abstractions Through Neuroimaging: The Neural Drift Diffusion Model. Psychological Review, 122, 2 (Apr 2015), 312-336.
[33] Plummer, M. JAGS: A program for analysis of Bayesian graphical models using Gibbs sampling City, 2003.
[34] Philiastides, M. G., Auksztulewicz, R., Heekeren, H. R. and Blankenburg, F. Causal role of dorsolateral prefrontal cortex in human perceptual decision making. Curr Biol, 21, 11 (Jun 07 2011), 980-983.
[35] Spiegelhalter, D. J., Best, N. G., Carlin, B. R. and van der Linde, A. Bayesian measures of model complexity and fit. J Roy Stat Soc B, 642002), 583-616.
[36] Hanks, T. D. and Summerfield, C. Perceptual Decision Making in Rodents, Monkeys, and Humans. Neuron, 93, 1 (Jan 04 2017), 15-31.
[37] Renninger, L. W., Verghese, P. and Coughlan, J. Where to look next? Eye movements reduce local uncertainty. J Vis, 7, 3 (Feb 27 2007), 6.
[38] Lederman, S. J. and Klatzky, R. L. Hand Movements - a Window into Haptic Object Recognition. Cognitive psychology, 19, 3 (Jul 1987), 342-368.
[39] Heekeren, H. R., Marrett, S., Ruff, D. A., Bandettini, P. A. and Ungerleider, L. G. Involvement of human left dorsolateral prefrontal cortex in perceptual decision making is independent of response modality. P Natl Acad Sci USA, 103, 26 (Jun 27 2006), 10023-10028.